frontiers | Frontiers in Marine Science

TYPE Original Research
PUBLISHED 25 August 2023
DOI 10.3389/fmars.2023.1167169

OPEN ACCESS

EDITED BY
Hiroaki Saito,
The University of Tokyo, Japan

REVIEWED BY
Yosuke Yamada,
Japan Agency for Marine-Earth Science and Technology (JAMSTEC), Japan
Marika Takeuchi,
University of Southampton,
United Kingdom

*CORRESPONDENCE
Shigeki Wada
swadasbm@shimoda.tsukuba.ac.jp

RECEIVED 16 February 2023
ACCEPTED 02 August 2023
PUBLISHED 25 August 2023

CITATION
Hayashi Y, Wada S, Seto M and Adachi Y (2023) Cohesive bond strength of marine aggregates and its role in fragmentation. *Front. Mar. Sci.* 10:1167169. doi: 10.3389/fmars.2023.1167169

Cohesive bond strength of marine aggregates and its role in fragmentation

Yasuhito Hayashi[1], Shigeki Wada[1]*, Mayumi Seto[2] and Yasuhisa Adachi[3]

[1]Shimoda Marine Research Center, University of Tsukuba, Shimoda, Shizuoka, Japan, [2]Department of Chemistry, Biology, and Environmental Sciences, Nara Women's University, Kita-Uoya Nishimachi, Nara, Japan, [3]Faculty of Life and Environmental Sciences, University of Tsukuba, Tsukuba, Ibaraki, Japan

Marine aggregates are one of the main contributors to carbon sequestration in the deep sea through the gravitational settling of biogenic particles formed from the photosynthetic products of phytoplankton. The formation of large particles due to aggregation processes has been the focus of studies in the past, but recent findings on the spatio-temporal distribution of particles suggests that the fragmentation of aggregates plays an important role in aggregate dynamics. Here, we assessed the yield strength of aggregates derived from natural planktonic communities in order to analyze the cohesive bond strength and further understand fragmentation. The experimental approach was designed around the use of a Couette device, which produces a constant laminar shear flow of water. Aggregates were found to have a higher yield strength (~289 ± 64 nN) during phases of nutrient depletion than those of mineral particles such as montmorillonite. Based on an estimated cohesive bond strength of 96 nN a numerical model to predict the temporal variation of aggregate size was created. The output of this model indicates that cohesive bond strength is a major determinant of the size of aggregates in motion. Our findings suggest that the dynamics of marine aggregates are greatly influenced by cohesive bond strength and the role in fragmentation.

KEYWORDS

marine snow, fragmentation, aggregate strength, cohesive bond strength, plankton

1 Introduction

In the world's oceans, phytoplankton is responsible for major part of the assimilation of inorganic carbon annually (Falkowski, 2012). Fixed organic carbon is partly exported to the deep ocean via gravitational settling, contributing to carbon sequestration (Alldredge and Silver, 1988; Boyd et al., 2019) and the energy supply of mesopelagic organisms (Irigoien et al., 2014; Uchimiya et al., 2018). Rapidly settling particles such as fecal pellets and amorphous aggregates formed by the adhesion of colloidal particles (Aggregates: 13-260 m d^{-1}; Laurenceau-Cornec et al., 2015a; Phytoplankton cells: 0.10-0.71 m d^{-1}; Oliver et al.,

1981; Fecal pellets: 50.8-155.2 m d^{-1}; Yoon et al., 2001) also have a role in carbon sequestration as carriers of organic carbon (Alldredge et al., 1987; Alldredge and Gotschalk, 1989; Passow et al., 1994; Turner, 2002, Turner, 2015). The amount of organic carbon transported to the deep ocean by gravitational settling was estimated to be 4.0-9.1 Pg y^{-1} (Siegel et al., 2014), accounting for 37-83% of anthropogenic CO_2 emission (10.9 ± 0.9 Pg C y^{-1}; IPCC AR6, 2021). Aggregates would be a carrier of organic carbon. In Kerguelen Plateau, the contributions of aggregates to the overall number and carbon of settling particles were estimated to be 49 ± 10 and 30 ± 16%, respectively (Laurenceau-Cornec et al., 2015b). Large contributions of aggregates were also observed in the study in Bermuda Atlantic, in which 72 ± 2 and 65 ± 5% of the total number of settling particles were derived from aggregates in spring and autumn, respectively (Cruz et al., 2021).

Aggregate size is one of the critical parameters for export process. Larger aggregates with higher settling velocity (Laurenceau-Cornec et al., 2015a) and larger carbon content (Alldredge et al., 1998) imply the importance of study on dynamics of aggregate. One of the important components of marine aggregates is extracellular polymeric substances produced by phytoplankton and bacteria (Alldredge et al., 1993; Passow et al., 1994; Alldredge et al., 1998; Passow, 2002b), with the highly adhesive property of EPS contributing to the cohesion of particles (Kobayashi, 2005; Chen et al., 2021; Quigg et al., 2021). Minerals and cells of organisms (e.g., phytoplankton and bacteria) would be also involved in the aggregate (Alldredge and Silver, 1988; Passow, 2002a). In addition, physical processes such as turbulence and differential sedimentation enhance collisions among particles driving aggregation (Saffman and Turner, 1956; Kepkay, 1994; Soos et al., 2008). While aggregation drives the enlargement of particles, the contrary process of fragmentation could coincide by relative fluid motion. Fragmentation inducing hydrodynamic forces occur via various processes such as turbulence in the surface layer, settling shear, and the movement of zooplankton (Hill, 1998; Winterwerp, 1998; Dilling and Alldredge, 2000; Hill et al., 2001; Goldthwait et al., 2004). For example, Takeuchi et al. (2019) suggests that the size of aggregates is limited by turbulent eddies based on a field observation conducted with a turbulence profiler and image analysis. Other recent findings on the spatio-temporal variations of particles also suggest fragmentation of aggregates occurs, such as Briggs et al. (2020) who found that the amounts of both small and large particles were seen to change at similar rates throughout the water column even though large particles have a faster settling rate than smaller particles.

Fragmentation of aggregates highly depends upon the bond strength between the comprising clusters of particles (Parker et al., 1972; Boller and Blaser, 1998; Kobayashi et al., 1999; Kobayashi, 2004). Adachi et al. (2019) reported a cohesive bond strength of 5 to 11 nN for clay particles (montmorillonite) under laminar shear flow generated using a Couette device, an apparatus which has been widely applied to assess the aggregation process of marine particles (Drapeau et al., 1994; Passow, 2000; Verspagen et al., 2006). However, the clay particles they used may have different fragmentation processes from particles originated from marine plankton. Experimental assessment of the fragmentation of aggregates collected from the ocean was first carried out by Alldredge et al. (1990). Based on an experiment using an oscillation grid to produce turbulence, they concluded that breakup is unlikely to occur under normal ocean conditions. On the other hand, another study using a rotating cylindrical tank to create intermittent periods of motion suggested that the fragmentation of aggregates originates from a cultured strain of diatoms at levels of shear flow found in natural environments (Song and Rau, 2022). We believe that the discrepancy seen between these two reports is due to either the method of sample collection (compacting), the underestimation of the hydrodynamic force exerted on marine aggregates due to non-uniform or intermittent fluid motion, or the difference in the cohesive bond strength of the analyzed particles (Alldredge and Silver, 1988; Song and Rau, 2022). In this study, we estimate the cohesive bond strength of aggregates formed by marine planktonic communities using the Couette device according to Adachi et al. (2019). Particles dispersed in a Couette device adhere under a stable laminar shear flow when the cohesive bond strength is high enough to withstand the fluid shear. However, as aggregates increase in size, aggregation is hindered by the increased influence of external forces. When the size of aggregates stabilizes in a system, the yield strength of the aggregates is equal to the hydrodynamic force of fluid shearing. In addition, a numerical model with cohesive bond strength as a function is used to predict the size of particles (Son and Hsu, 2009), enabling us to assess the impact fragmentation has on the dynamics of organic marine aggregates.

2 Materials and methods

2.1 Theory

Fragmentation occurs when the hydrodynamic force [F_{hyd} (nN)] exceeds the yield strength of an aggregate (F_{agg})(Kobayashi, 2004). When the size of an aggregate is smaller than Kolmogorov microscales, F_{hyd} is expressed by the following equation (Blaser, 2002):

$$F_{hyd} = C_{hyd}\mu G\frac{S}{2}, \quad (1)$$

where C_{hyd}, μ, G, and S denote the constant depending on the axial ratio and aggregate orientation (dimensionless), viscosity of seawater (0.959×10^{-3} kg m^{-1} s^{-1}, Sharqawy et al., 2010; Nayar et al., 2016), shear rate (s^{-1}), and surface area (m^2), respectively (all values to calculate F_{hyd} were listed in Table S1). Under the assumption that the aggregates are ellipsoidal, we used a value of 1.25 for C_{hyd} based on Blaser's estimation (Blaser, 2002; Frappier et al., 2010). Aggregation is accelerated by fluid motion through the heightened number of collisions among particles. However, an increase in size leads to fragmentation as a consequence of the hydrodynamic force on aggregates being proportional to their surface area (eq.1). Under constant fluid motion, the size of aggregates is expected to plateau when F_{agg} is equal to F_{hyd}. In the present study, we used 99% cumulative size [D_{99} (μm)] at the time of plateau to calculate F_{agg} as recommended by Adachi et al. (2019).

Aggregates consist of clusters of particles, and the yield strength of aggregates is the product of the number of points of contact and the bond strength between clusters (N_c and F_{coh}, respectively) (Kobayashi et al., 1999):

$$F_{agg} = N_c \times F_{coh} \quad (2)$$

2.2 Incubation of natural planktonic community

Surface seawater was collected from Nabeta bay, Shizuoka, Japan (34.67N, 138.93E, Water depth: 3m, Supplementary Figure S1), in August 2020 using a plastic bucket. In the previous study, predominance of diatom and dinoflagellates were found in this region (Hama et al., 2012; Hama et al., 2016). After filtering the seawater with a 100 µm mesh to remove large particles, the phytoplankton were remediated with nutrients (final concentration; $NaNO_3$ and KH_2PO_4: 8.85 and 0.55 µM). Samples of the seawater (20L) were transferred into seven transparent tanks (20 L polycarbonate) and kept within an uncovered outdoor aquarium. Fresh seawater was continuously pumped to the aquarium from Nabeta bay to maintain *in situ* water temperature. The water temperature (INFINITY-CTW(ACTW-USB), JFE Advantech, Inc.) and photon flux of the samples (DEFI2-L, JFE Advantech, Inc.) were monitored at 1-minute intervals over the course of the experiment. The planktonic community incubation period was 6 days, with subsamples collected on days 0, 2, 4, and 6. Two tanks were retrieved on each experimental day except for day 0 (single tank was used). Approximately 14 L of subsamples from each tank were utilized for the aggregation/fragmentation experiment as described later. A small portion of each subsample (50 ml) was fixed with glutaraldehyde (final concentration: 1%) and temporarily stored at 4°C until analysis of bacterial abundance could be conducted. Excess water (900-1200 mL) not utilized in the aggregation/fragmentation experiment was filtered through glass fiber filters (GF/F, Whatman). The filters and filtrates were stored in acid-cleaned polycarbonate bottles and frozen at -20°C.

2.3 POC, chlorophyll *a*, nutrient concentration and bacterial abundance

The POC concentration of the samples was determined with an Elemental analyzer (FlashSmart, Thermo Fischer) after the removal of inorganic carbon with HCl vapor. Chlorophyll *a* was extracted with *N,N*-dimethylformamide in accordance with Suzuki and Ishimaru (1990), and its concentration was quantified with a fluorometer (F7000, HITACHI) (Welschmeyer, 1994). Nutrient concentrations in the filtrates were measured using an autoanalyzer (Quattro, BL-tech) as per Hama et al. (2016). For this study, the sum of nitrate, nitrite and ammonium is expressed as Dissolved Inorganic Nitrogen (DIN). The bacterial cell count was enumerated with an epifluorescent microscope (BX53; Olympus) after staining the cells with 4',6-diamidino-2-phenylindole (DAPI) (Shimotori et al., 2009).

2.4 Montmorillonite particles

For authentic standard, purified montmorillonite (Kunipia-F, Kunimine Co. Ltd) was added to a 1.0 M NaCl solution and dialyzed (Cellulose Tubing (36/32), Viskase Companies Inc.) to a level of conductivity less than 2.0 uS cm^{-1} as recommended by Adachi et al. (2019). The stock solution was then diluted with artificial seawater (MARINE ART SF-1, Tomita Pharmaceutical) to a concentration of 0.5-1 mg L^{-1}. Initial size of the motmorillonite flocs were 1630 ± 450 (mean ± SD) µm.

2.5 Aggregation/fragmentation experiment

A constant laminar shear flow was generated with a Couette device, which consists of two concentric cylinders with a rotating outer cylinder and stationary inner cylinder (Drapeau et al., 1994). The inner diameter of outer cylinder and outer diameter of inner cylinder were 115 and 90 mm respectively (distance between cylinders: 12.5 mm), and the horizontal length of the device was 256 mm. The outer cylinder was connected to an induction motor (M315-401, Oriental motor) to generate rotation. The shear rate G (s^{-1}) between the two cylinders is a function of the speed of rotation as seen below:

$$G = \frac{2\pi NR}{60d}, \quad (3)$$

where N, R and d denote rotation speed (rpm), inner radius of the outer cylinder (m), and the distance between cylinders (m), respectively. The space between the cylinders was filled with 1.5 L of seawater, and a laminar shear flow (3.4, 7.2, 10.6, 14.5 and 22.6 s^{-1}) was generated by rotating the outer cylinder at 7, 15, 22, 30, and 47 rpm, respectively, for 120-180 min.

2.6 Visualization and image analysis

The seawater within the Couette device was illuminated by a LED slit light (LA-HDF 158A, HAYASHI-REPIC) positioned 10 cm vertically above the apparatus. With a digital camera affixed perpendicularly to the light source, we photographed the region of 52.4 × 34.9 mm at distance of 20 cm from the sensor. To determine the size of particles, we used polystyrene beads with a diameter of 650 µm (MORITEX 4365A), which were dispersed in the Couette device. We randomly selected 153 beads in focus, and those were analyzed using the Fiji segmentation editor (Schindelin et al., 2012). The mean value of the size normalized by pixels was 8.52 µm/pixel. The error in the visualization process was 0.5 µm (standard deviation of the size of 153 beads) probably due to depth of field.

Burst shots with 22-56 consecutive pictures were taken with a camera (SONY a6300 with SEL50M28, Figure 1) at fixed intervals of 5 or 10 minutes with 3-11 frames sec^{-1}. To evaluate the bias due to recounting same aggregates in the continuous frames, we split the dataset every three frames. Assuming that aggregates moved with rotation of the outer cylinder, most of aggregate would move out of the frame after 3 frames. The sizes of aggregates calculated from

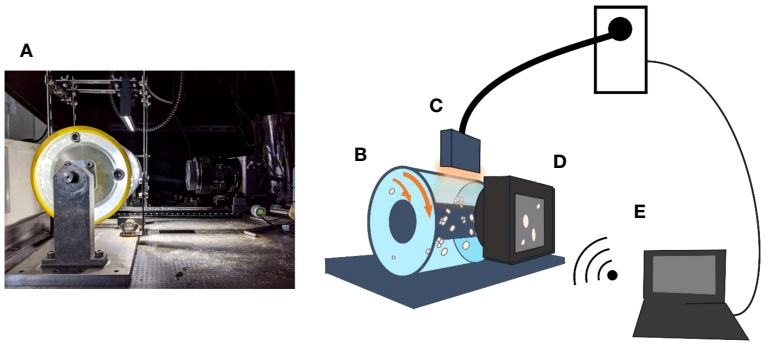

FIGURE 1
Experimental setup **(A)**. Aggregate growth in the Couette device **(B)** was illuminated with an LED slit light **(C)** and captured by a camera **(D)**. Both the LED light and camera were controlled remotely **(E)**.

split dataset were 84-105% of those from whole one (Supplementary Figure S2). Due to problem of setting for camera, we did not collect the data in the treatment with 15 rpm on day 6.

First, the brightness of the images was normalized with a mean and standard deviation of 64 and 32, respectively. The images were then processed to remove noise and artifacts caused by distortion, brightness gradients, scratches on the inner cylinder, and out of focus objects. Only the central region (3400 × 6000 pixels) of the images were utilized to avoid the heavily distorted areas caused by the convex surface of the outer cylinder. For each set of images, the positions of the particles suspended in the seawater are variable, while brightness gradients due to the angle of illumination and scratches on the inner cylinder remain constant. To remove these irregularities, the median brightness for a set of images was subtracted from each image.

The spatial frequency spectra of the images were obtained with a Fast Fourier Transformation (FFT), and a high pass filter was applied to remove any out-of-focus objects. This approach was modified the method in the previous study (Spinewine et al., 2003). The spectra were then transformed into images via reverse FFT (Figures 2A, B), and the newly created images were treated as the base images for analysis. Finally, binarization was conducted on the base images at a predetermined threshold value (20 in this experimental setting). The validity of the threshold was tested by comparing the images processed with different threshold values (Supplementary Figure S3).

A neural network model (Transfer Learned from YOLOv5s) was utilized on the base images to detect particles (Jocher et al., 2021). In the case of overlapping particles, the particles were dissociated by a watershed algorithm (Figure 2C) (Kowal et al., 2020). The projected area, major and minor axes, and length of perimeter of each particle were estimated with the regionprops_table from the scikit-image Python library (van der Walt et al., 2014), and the surface area of the particles (S in equation 1) was calculated using major and minor axes in accordance with Adachi et al. (2019). We determined the minimum detection limit to be 2000 pixels based on a comparison of the images among different levels of detection limits (1000, 2000 and 5000 pixels). The particles detected in the size of 1000-2000 pixels had more blurred ones than those of 2000-5000 and more than 5000 pixels (Supplementary Figure S4). In addition, calculated F_{hyd} values were constant over 2000 pixels (Supplementary Figure S5) probably because of inclusion of particles which were not aggregates in the range of smaller size. In this study, aggregates with an extremely high or low solidity, a high aspect ratio, or a projected surface area less than 2000 pixels were removed from the images. Particle numbers visualized each time period were different among rotation speeds (53 ± 28 particles for 7 rpm, 270 ± 109 for 15 rpm, 516 ± 275 for 22 rpm, 703 ± 533 for 47 rpm), because small number of larger aggregates were formed in the lower rotation speed. The numbers of analyzed montmorillonite particle were 2165 ± 146, 2507 ± 897, 382 ± 117 and 390 ± 182 at rotation speeds of 7, 15, 22, 30 rpm, respectively.

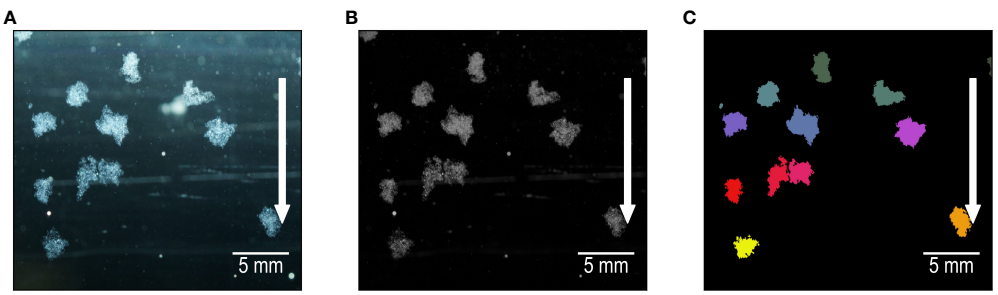

FIGURE 2
Image processing: **(A)** Original, **(B)** Base, and **(C)** Processed image. Scale bars show 5 mm. The white arrows indicate the direction of flow within the Couette device.

3 Results

3.1 Incubation of natural planktonic communities

For each day of the incubation period, the peak values for solar irradiance ranged from 1982-2444 µmol photons m^2 s^{-1} (Figure 3A) and water temperature of the aquarium ranged from 21.8 to 26.8°C (Figure 3B). The POC concentration increased from 25.8 µM on day 0 to 86.1-89.8 µM on day 2, but then decreased to 43.4-45.7 µM by day 6 (Figure 3C). Chlorophyll *a* showed no clear peak during the incubation period, with values ranging from 1.18 to 4.66 µg L^{-1} (Figure 3D). DIN concentration drastically declined from 8.31 µM on day 0 to 1.3 µM on day 2 and remained at a low concentration ranging from 0.66-1.15 µM for the rest of the incubation period (Figure 3E). Dissolved inorganic phosphorus (DIP) concentrations declined from 0.37 µM on day 0 to under the detection limit on day 2. By day 6, the values had slightly increased to a range of 0.07-0.10 µM (Figure 3F). Bacterial abundance was 0.78 × 10^7 cells mL^{-1} on day 0, and the maximum abundance of 2.8 × 10^7 cells mL^{-1} was found on day 6 (Figure 3G).

3.2 Aggregates in the laminar shear flow

It is difficult to avoid disturbance when the samples are introduced into Couette device. Therefore, the size distribution at the starting point could be variable, but such disturbance would not theoretically affect the D_{99} values in plateau phase. Plateaus in aggregate size were identified by fitting the D_{99} with a sigmoidal

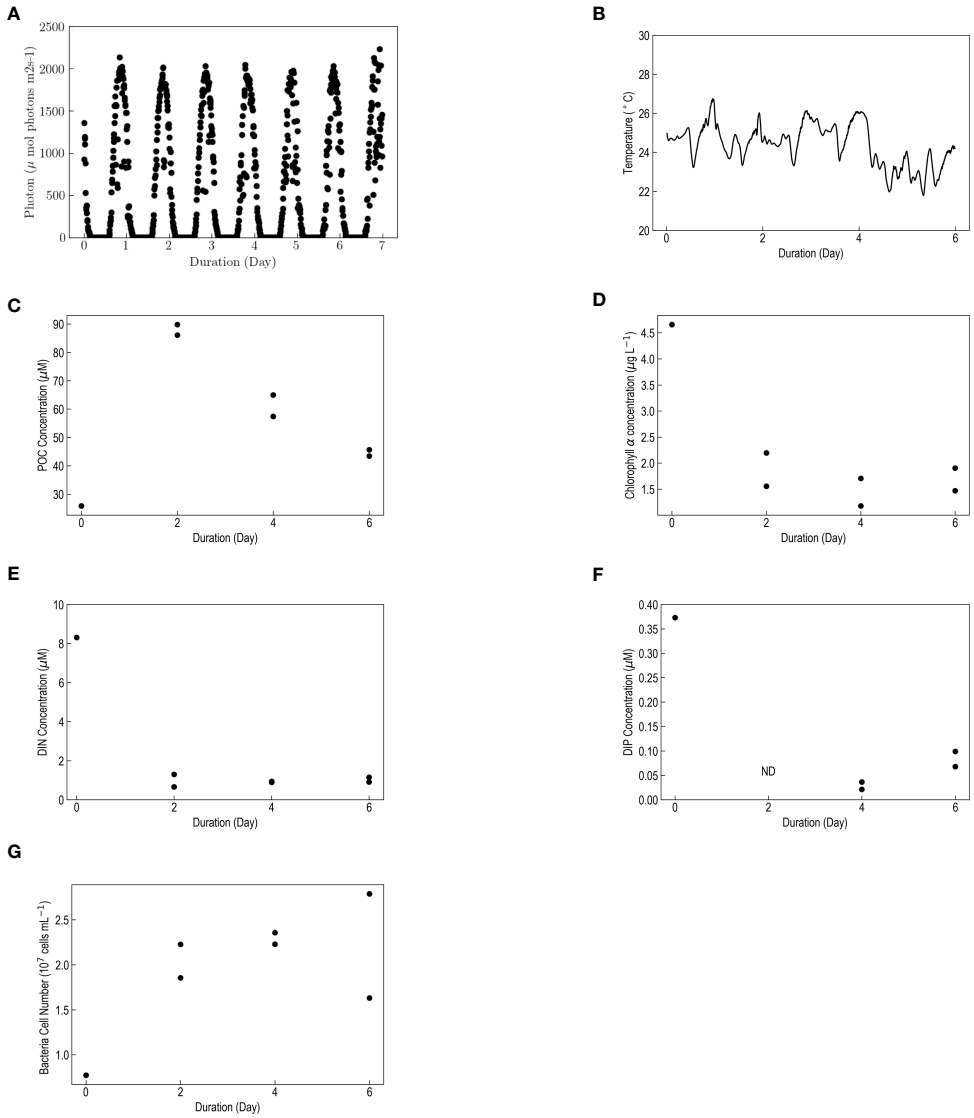

FIGURE 3
(A) Photon irradiance, **(B)** Temperature, **(C)** POC concentration, **(D)** Chlorophyll a concentration, **(E)** DIN concentration, **(F)** DIP concentration, **(G)** Bacterial cell count *vs.* incubation duration (Days). Two points for one day **(C-F)** indicates replicate samples (n = 2) except for day 0 (single sample). ND in **(F)** indicates not detected.

curve (Figure 4). For this experiment, the beginning of a plateau was defined as the time-point where the fitting curve reaches 95% of the maximum value for aggregate size. For the planktonic community water samples, on day 0 there were no aggregates with a projected surface area of larger than 2000 pixels detected under any shear conditions; however, an increase in aggregate size was noticed on day 2. The D_{99} of aggregates at the time of plateau on days 2, 4 and 6 ranged 3310-6840, 2980-8250, and 3750-9230 µm, respectively. The D_{99} at the lowest rotation speed (7 rpm) were 6840, 8200-8250 (duplicate samples) and 9230 µm on day 2, 4, 6, while those values declined to 3310, 2790-2980 and 3750-4050 µm under maximum speed (47 rpm), respectively (Figures 4, 5). For the montmorillonite sample, aggregates were observed to form at a faster rate compared to planktonic samples, ranging 11-36 minutes (Figure 6) probably due to dependency of montmorillonite on concentrations of electrolytes (Furukawa et al., 2009). The D_{99} of the montmorillonite aggregates ranged from 1920-4650 µm, and an overall smaller size was observed under higher rpm.

4 Discussion

4.1 Culture of natural planktonic communities

An increase in POC concentration from day 0 to day 2 coincided with a decrease in nutrients, suggesting a stimulatory effect of nutrients on the growth of phytoplankton; however, the highest concentration of chlorophyll *a* was observed on day 0. Although it was unexpected that peak of chlorophyll a was not appeared, we speculate that chlorophyll *a* concentration was greatest between day 0 and day 2 because it is a highly labile pigment. The presence of a chlorophyll *a* peak within a short incubation period (1-2 days) was also found in previous studies where natural phytoplankton communities were collected in the same manner as the present study (Hama et al., 2016). Bacterial cell counts showed a rapid increase by day 2, suggesting that POC production by the phytoplankton had a positive effect on bacteria reproduction as well as other mesocosm studies (Smith et al., 1995; Duarte et al., 2005).

4.2 Aggregate strength

As described above, the beginning of a plateau was defined as the time-point where the fitting curve reaches 95% of the maximum value for aggregate size, and we assume that size distribution is constant during the plateau. To confirm the presence of a plateau in aggregate size, the period of an apparent plateau (beginning of plateau to the end of the experiment) was divided evenly into the two phases of "Former" and "Latter". Using these phases, we evaluated the dynamics of particles based on size distribution (Figures 7, 8). There was no evident shift in cumulative frequency from "Former" to "Latter" phases except for the data with treatment of 7 rpm on day 2 (Supplementary Table S1), indicating that the dynamics of particles driven by a balance of aggregation and fragmentation would be stable during a period of plateau in aggregate size.

A homogenous structure is required to estimate the yield strength of an aggregate. Homogeneity can be evaluated based on

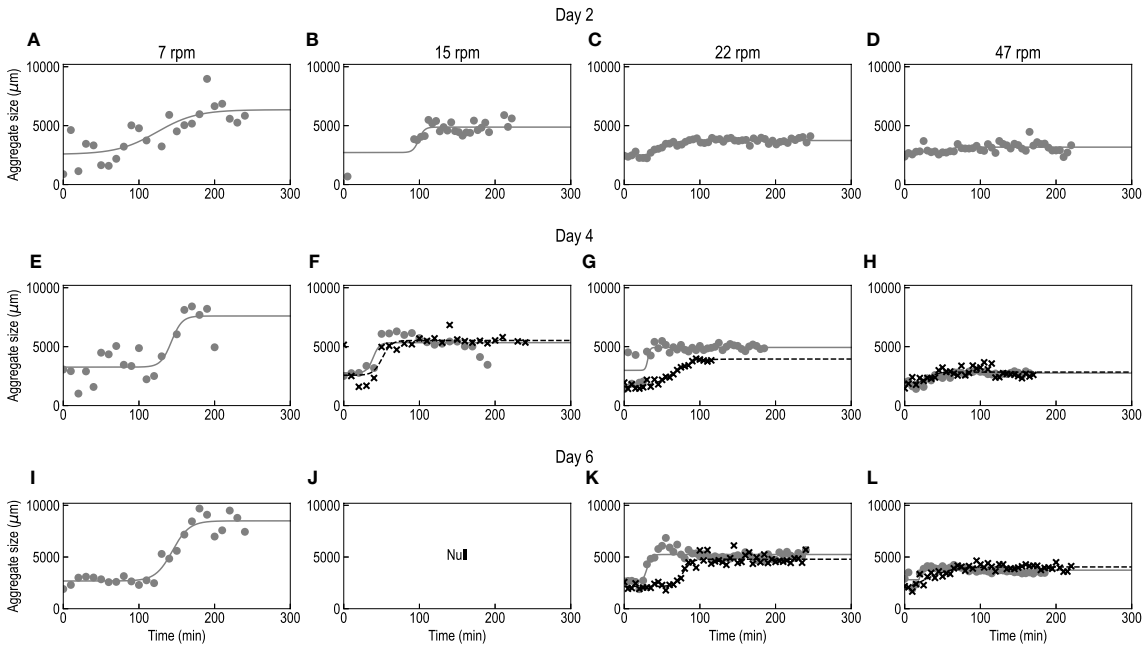

FIGURE 4
Time evolution of the aggregate size (D_{99}) for the aggregation/fragmentation experiment conducted on days 2 **(A–D)**, 4 **(E–H)** and 6 **(I–L)** at rotational speeds of 7 **(A, E, L)**, 15 **(B, F, J)**, 22 **(C, G, K)**, and 47 **(D, H, L)** rpm. Gray and black crosses indicate duplicate samples, and the curves are sigmoidal fitting. Null indicates that no data is available.

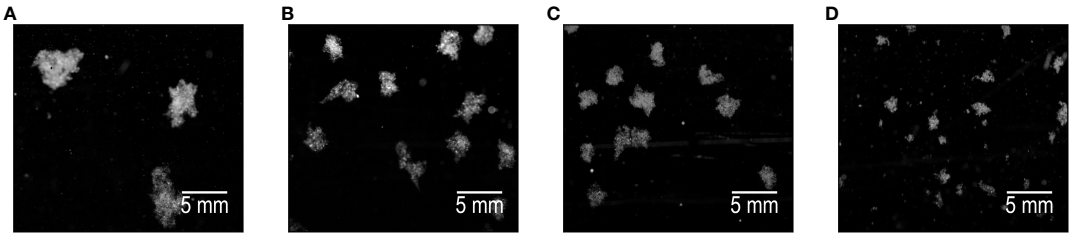

FIGURE 5
Typical images of aggregates at each level of shear rate [**(A)** 7, **(B)** 15, **(C)** 22 and **(D)** 47 rpm] on day 4.

a constant γ with the following equation:

$$D \sim G^{\gamma} \quad (4)$$

where D is the diameter of the aggregates (μm). In equation 4, a value of γ near -0.5 implies a homogeneous structure of the aggregates (Adachi et al., 2019). Because the value of γ was not consistent between replicate samples on day 2 (tank 1: not detected, tank 2: γ= -0.42), we did not include the data from day 2 in further analysis. In the present study, the γ values on day 4 and 6 were estimated to be -0.54 ± 0.04 and -0.47 ± 0.03 ($p<0.001$, GLM), respectively (Figure 9). The γ value of the montmorillonite particles was -0.54 ± 0.09 ($p<0.001$) (Figure 10), suggesting homogeneous structure of both aggregates under the different shear conditions.

Equation 1 was used to estimate the yield strength of the aggregates using surface area of aggregates (S (m^2)) which was calculated by the following equation (Adachi et al., 2019):

$$S = 2\pi\left(a^2 + \frac{(a)(b)^2}{\sqrt{b^2-a^2}}\arccos\left(\frac{a}{b}\right)\right), \quad (5)$$

where a and b are a half of minor and major axes (m), respectively.

The lack of aggregates detected on day 0 implies that size of aggregates was smaller than the detection limit (projected area: 2000 pixels). Assuming an ellipsoid with a ratio of 1:2 between the minor and major axis, minimum detectible size was a particle with a major axis length of 312 μm. Assuming yield strength was the limiting factor restricting aggregate growth, the yield strength for day 0 was estimated to be 6.5 nN. For samples from days 4 and 6, the yield strength of the aggregates was determined to be 213 ± 39 and 289 ± 64 nN, respectively. Our results suggest that the yield strength of aggregates was higher in the latter stages of incubation when a depletion of nutrients and an increase in bacterial abundance were observed (Figures 3E–G). One of the potential contributors to the strength of marine aggregates are EPS, which form cross-linked structures between particles. Phytoplankton and bacteria are considered to be major producers of EPS in marine environments (Alldredge and McGillivary, 1991; Passow, 1991, Passow 2002a; Thornton, 2002; Yamada et al., 2016; Mari et al., 2017). Previous studies have demonstrated that both nutrient depletion stimulates EPS production in phytoplankton (Passow and Alldredge, 1995), and EPS secretion from bacterial growth can enhance aggregation (Yamada et al., 2016). However, relationship between EPS production and strength of aggregates is still unknown, because EPS production and their physicochemical property (e.g., stickiness) would be highly variable among species of phytoplankton and bacterial decomposition (Passow 2002a; Mari et al., 2017).

The yield strength of aggregates from the planktonic communities was approximately 3-5 times higher than that of montmorillonite aggregates (57 ± 20 nN) and similar to the activated sludge seen in a previous study (120-380 nN: Yuan and Farnood, 2010). It has been reported that the fibrous frame structure of bacterial EPS contribute to a high flocculant strength in activated sludge (Droppo, 2004). Additionally, fibrous structures have also been documented in marine aggregates (Alldredge and Silver, 1988), suggesting EPS contribute to the dynamics of marine aggregates. Strengths of marine aggregates were assessed to be from 10^{-1} to 10^{-5} N m^{-2} by a previous study (Song and Rau, 2022) in which aggregates originated from cultured phytoplankton were formed by differential sedimentation in a roller table. Assuming major and minor axes as 3 and 0.86 mm (medians of the size distribution of major axis and aspect ratio (3.5) in their study), respectively, yield strengths of the aggregates in Song and Rau (2022) were calculated to be 0.0202-202 nN. Relatively higher

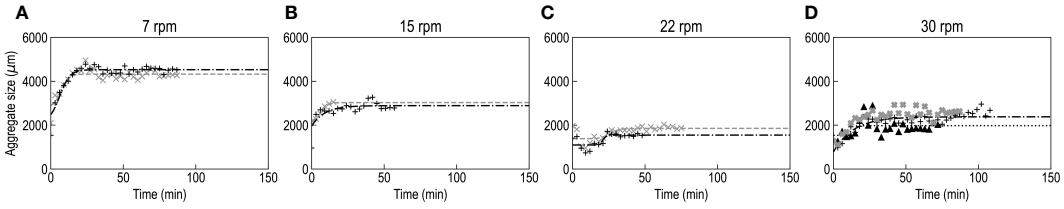

FIGURE 6
Time evolution of the aggregate size (D_{99}) for montmorillonite at rotational speeds of **(A)** 7, **(B)** 15, **(C)** 22, and **(D)** 30 rpm.

10.3389/fmars.2023.1167169

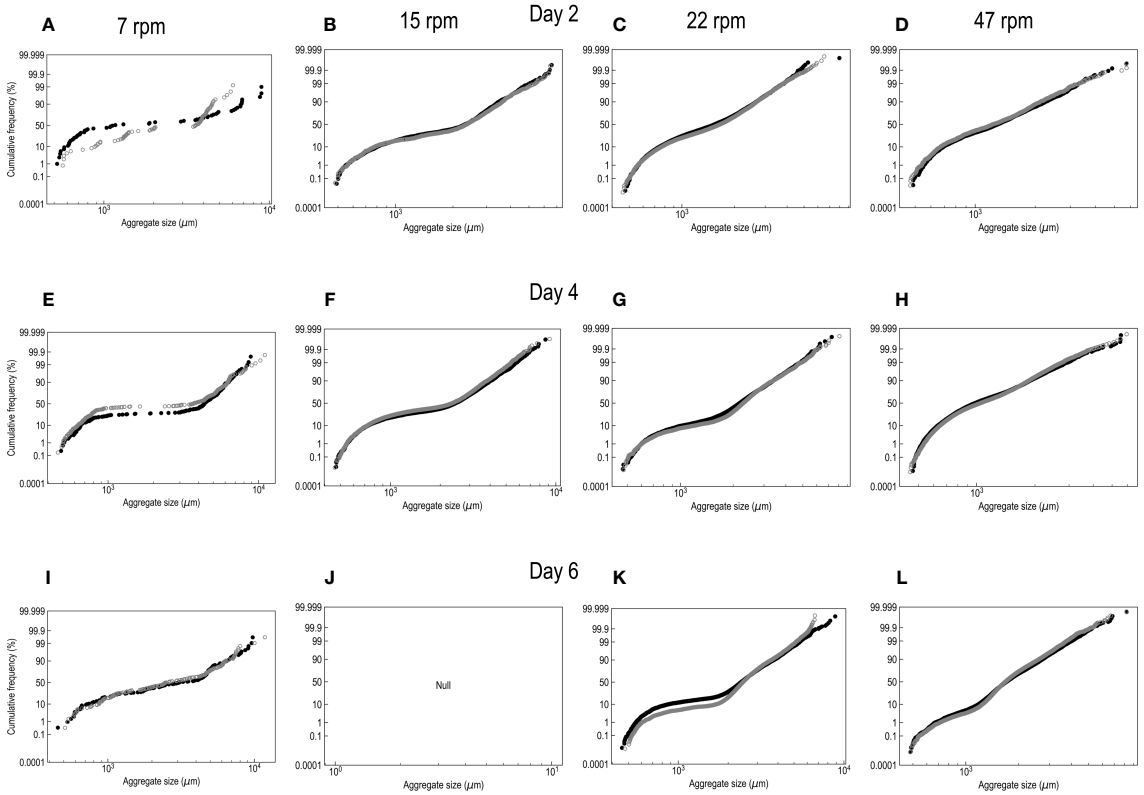

FIGURE 7
Particle size distribution for the aggregation/fragmentation experiment on days 2 **(A–D)**, 4 **(E-H)** and 6 **(I-L)** at rotational speeds of 7 **(A, E, I)**, 15 **(B, F, J)**, 22 **(C, G, K)**, and 47 **(D, H, L)** rpm. Black and gray circles indicate the data from the phases of "Former" and "Latter", respectively.

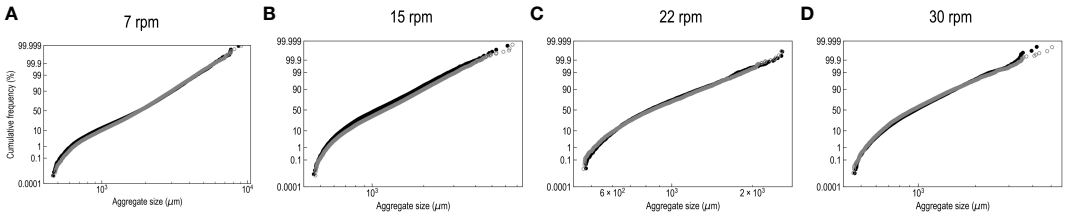

FIGURE 8
Particle size distribution for the aggregation/fragmentation experiment on montmorillonite particles at rotational speeds of 7 **(A)**, 15 **(B)**, 22 **(C)**, and 30 **(D)** rpm. Black and gray circles indicate the data from the phases of "Former" and "Latter", respectively.

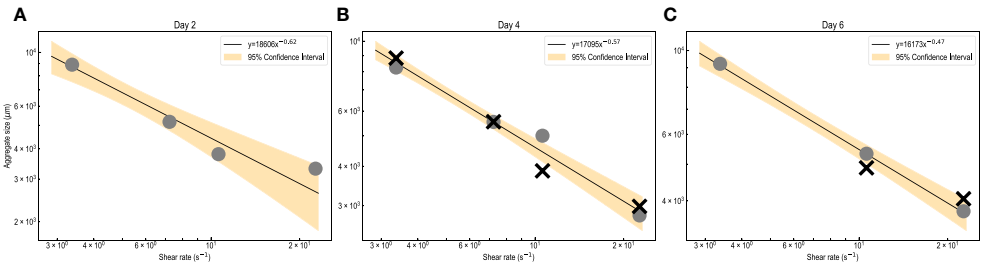

FIGURE 9
D_{99} (μm) as a function of shear rate (s^{-1}) for particles derived from planktonic communities on days **(A)** 2, **(B)** 4 and **(C)** 6. Gray and black crosses differentiate replicate samples. The curve and 95% confidence interval were calculated using exponential fitting.

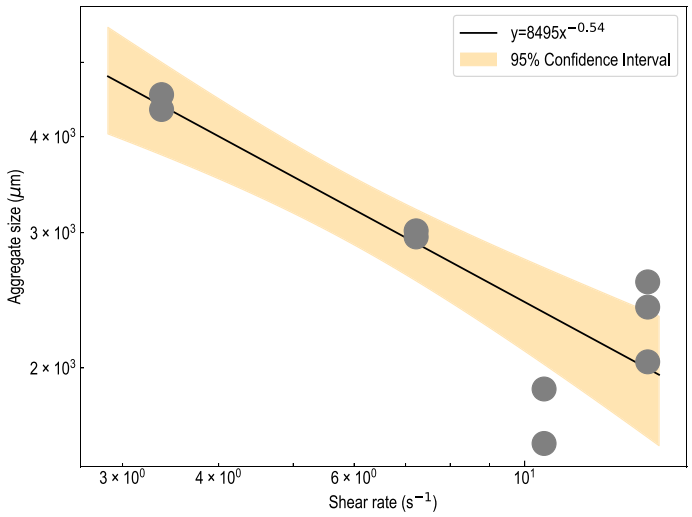

FIGURE 10
D_{99} (μm) as a function of shear rate (s^{-1}) for montmorillonite particles. The curve and 95% confidence interval were calculated using exponential fitting.

strength of marine aggregates in the present study might be also relevant with nutrient condition. Since phytoplankton in Song and Rau (2022) would be cultured with sufficient nutrients, EPS could be produced with lesser extent than the present study.

4.3 Cohesive bond strength

Adachi et al. (2019) calculated the N_c of montmorillonite flocs to be 3 points of contact based on 3D fractal dimensioning as described by Miyahara et al. (2002). Considering that the experimental setting in Adachi et al. (2019) was same as that in the present study, the same value for the N_c of montmorillonite was applied here. Although the 3D fractal dimension of aggregates from the natural planktonic communities was not evaluated in the present study, the perimeter-based 2D fractal dimension was calculated to serve as a reference for the aggregate structure (Florio et al., 2019) and determined to be 1.38 ± 0.03. This value is analogous to that of montmorillonite (1.39 ± 0.01) suggesting a structural similarity between the aggregates (Florio et al., 2019). Although the 2D fractal dimension could not always reflect structural properties, we assumed the N_c of aggregates from the natural planktonic communities to be the same as that of montmorillonite aggregates. The cohesive bond strength of aggregates from days 4 and 6 were estimated using equation 2 to be 71 ± 13 and 96 ± 21 nN respectively, and the cohesive bond strength of montmorillonite was estimated to be 19 ± 6.3 nN.

4.4 Effect of cohesive bond strength on aggregate size

Here, we applied a single-size-class aggregate growth model by Son and Hsu (2009) to evaluate the dependency of aggregate size on cohesive bond strength based on the assumption that the aggregate size is smaller than the turbulent eddy size:

$$\frac{dD}{dt} = \frac{D_p^{\beta}}{\beta \ln(D/D_p)+1}\left(\underbrace{\frac{K_a}{3}\frac{C}{\rho_s}D_p^{F}D^{-F+4-\beta}}_{Aggregation} - \underbrace{\frac{K_b}{3}\left(\frac{\mu G}{(\pi/6)^{-2/3}\times F_{coh}}\right)^{q} D_p^{p+(2q/3)F}D^{1-\beta+(2q/3)(3-F)}(D-D_p)^{p}}_{Breakup}\right) \quad (6)$$

According to this model, cohesive bond strength (F_{coh}) is only involved in fragmentation and not involved in aggregation (equation 6). D, D_p, C, ρ_s, and F are the aggregate size, primary particle size, concentration, primary particle density, and fractal dimension, respectively. β is the coefficient relevant to the fractal dimension, p and q are empirical coefficients. K_a and K_b are the fitting parameters for aggregation and fragmentation efficiency. For β, F, D_p, and ρ_s, we used -0.1, 2.0, 5×10^{-6} and 2650 as defined in previous studies using clay particles (Maggi, 2007; Son and Hsu, 2009). The experimental conditions ($D_{0\ =}$ 1356×10^{-6} m, $G = 3.4\ s^{-1}$, $C = 30 \times 10^{-3}$ g L^{-1}, F_{coh} = 19 nN), and data from the experiment performed on montmorillonite (Figure S6: 7 rpm) were used to calculate K_a and K_b. For this calculation, the ranges for K_a and K_b in the previous study (0.07-6.74 and 0.0756-2.95 $\times 10^{-5}$, respectively; Son and Hsu, 2009) were modified (0.01-10 and 1×10^{-6}-0.01, respectively in the present study), and the K_a and K_b values that minimize the residual sum of squares for the experimental data were estimated with a Python curve-fit to be 0.86 and 8.3×10^{-4}, respectively.

The values of ρ_s and F of particles in seawater were set to 1052 and 1.8, respectively (Kahl et al., 2008; Laurenceau-Cornec et al., 2015a). The concentration of particles was set to a value observed in a coastal region in Tokyo Bay, Japan ($C = 5.0 \times 10^{-3}$: Ahrens et al., 2010), and 50 μm was used as the initial size of the aggregate. Using these parameters, we calculated the time evolution of aggregate size in the ocean (Figure 11A). In the present study, experimental approach was carried out by using seawater samples collected in Shimoda, but phytoplanktonic communities were spiked with nutrients. Therefore, we referred the concentration of particles in

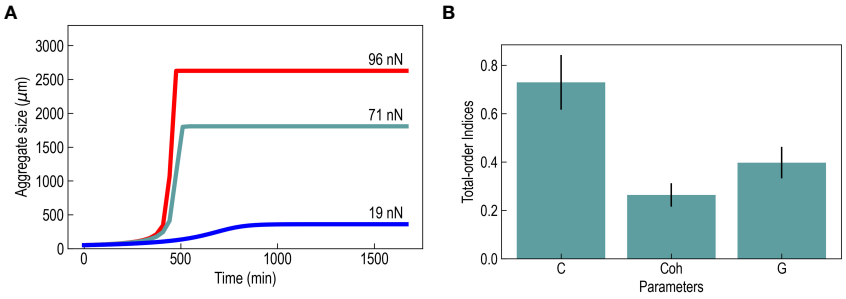

FIGURE 11
(A) Size of a marine aggregate with a cohesive bond strength of 20, 72 and 98 nN (values of montmorillonite, planktonic particles on day 4 and planktonic particles on day 6, respectively) as a function of time (min) predicted by the numerical model, and **(B)** total-order Sobol's indices for *C*, F_{coh} and *G* The error bars imply a 95% confidence interval.

Tokyo Bay for the numerical model, because it is well known as an eutrophic region (Furukawa and Okada, 2006).

Aggregate sizes ranged from 360-2627 μm with a range of cohesive bond strengths of 19-96 nN (Figure 11A). We performed a Sobol' sensitivity analysis (Usher et al., 2016) to determine the model's sensitivity to *C*, *G*, and F_{coh} with the ranges of 1-10 mg L^{-1}, 0.2-1 s^{-1} and 19-96 nN, respectively. Total-order Sobol's sensitivity indices of *C*, *G*, F_{coh} were 0.73 ± 0.10, 0.26 ± 0.04, and 0.40 ± 0.06, respectively, showing that these three parameters are important determinants of the size of aggregates (Figure 11B). To examine the sensitivity of aggregates to varying levels of F_{coh}, we evaluated the model at several fixed points for *G* (0.2, 0.4, 0.6, 0.8, 1.0 s^{-1}) and *C* (1, 3, 5, 7, 10 mg L^{-1}). Comparing aggregates at the minimum F_{coh} (19 nN), and at the maximum (96 nN), there was a size difference of 320-750%, revealing that the size of an aggregate is highly dependent on F_{coh} (Figure 12). Estimation of cohesive bond strength allowed us to use single-size-class aggregate growth model to show the aggregate dynamics.

We extract the data of settling velocity and particle size in case of 3D fractal dimension at 1.8 from Laurenceau-Cornec et al. (2015a) with WebPlotDigitizer (Rohatgi, 2022), and empirical formula were provided as below;

$$U = 64.7\ D^{-0.58}, \tag{7}$$

where *U* and *D* were terminal settling velocity (m d^{-1}) and particle size (μm), respectively. The settling velocities at the aggregates size of 360 and 2627 μm (aggregate size in case of F_{coh} at 19 and 96 nN) were calculated to be 36 and 113 m d^{-1}, and the time scales of the aggregates in the euphotic zone (200 m) were 5.7 and 1.8 days, respectively. Since settling particles would be decomposed by heterotrophic bacteria with time scales of days to weeks (0.04-0.286 d^{-1}; Iseki et al., 1980; Goutx et al., 2007), variability of F_{coh} could be a determinant of export ratio.

The significance of fragmentation in the dynamics of marine aggregates remains a matter of controversy. Alldredge et al. (1990) experimentally tested the fragmentation process and concluded that aggregates would not yield to the hydrodynamic forces present in marine environments. Comparison with output of numerical model in the present study also showed higher strength of aggregates in Alldredge et al. (1990) (Figure 12). We considered such discrepancy is attributed to sampling method. She collected aggregates by hand, but the structure of aggregates could be modified in sampling (e.g., compacting; Alldredge and Silver, 1988). On the other hand, recent field surveys on the size distribution of particles suggest fragmentation occurs throughout the water column (Takeuchi et al., 2019; Briggs et al., 2020). The higher cohesive bond strength of biogenic particles compared to montmorillonite as seen in this study, and similar to the reported aggregate strength

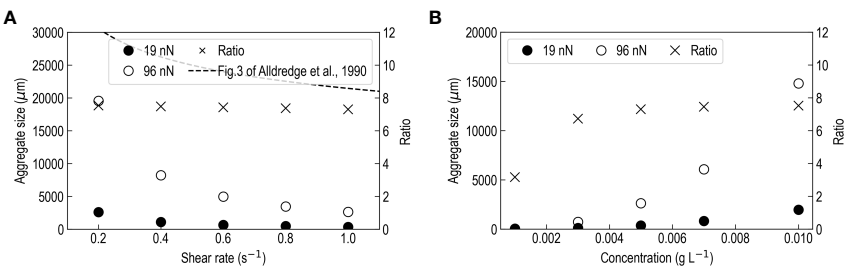

FIGURE 12
The predicted size of aggregates at several levels of **(A)** shear rates and **(B)** particle concentrations with high and low cohesive bond strengths (20 and 98 nN). Ordinates show aggregate size, and abscissa show shear rate (s^{-1}) and particle concentration (mg L^{-1}). The ratio of the estimates at a cohesive bond strength of 98 nN against that of 20 nN are plotted as black crosses. The concentration in panel **(A)** and shear rate in panel **(B)** were fixed to be 5 mg l^{-1} and 1 s^{-1}, respectively.

of activated sludge suggests that organic matter such as EPS act as a bio-flocculant among particles. In future, it will be required to determine the group of organisms affecting aggregate strength. The results of this research demonstrate that the analysis of both the physical and biological processes present in marine environments is necessary to shed light on the dynamics of organic marine aggregates.

Data availability statement

The raw data supporting the conclusions of this article will be made available by the authors, without undue reservation.

Author contributions

YH, SW, and YA conceived and designed the experiments. YH performed the lab experiments and analyzed the data. YH and MS conducted the model experiments. YH wrote the manuscript with support from SW, MS, and YA. All authors contributed to the article and approved the submitted version.

Funding

This work was supported by JSPS Kakenhi program (16H06382, 21J20420, 22H00387), and Sasakawa Scientific Research Grant from the Japan Science Society (2019-6044).

Acknowledgments

We express thanks to all staff at Shimoda Marine Research Center for their kind help. We are also grateful to Drs. T. Hama and Y. Omori for their consultation and suggestions on this study. We would also like to thank George Northen from G-Horizon for their English review and consultation.

Conflict of interest

The authors declare that the research was conducted in the absence of any commercial or financial relationships that could be construed as a potential conflict of interest.

Publisher's note

All claims expressed in this article are solely those of the authors and do not necessarily represent those of their affiliated organizations, or those of the publisher, the editors and the reviewers. Any product that may be evaluated in this article, or claim that may be made by its manufacturer, is not guaranteed or endorsed by the publisher.

Supplementary material

The Supplementary Material for this article can be found online at: https://www.frontiersin.org/articles/10.3389/fmars.2023.1167169/full#supplementary-material

References

Adachi, Y., Di, C., Xiao, F., and Kobayashi, M. (2019). Size, orientation, and strength of Na-montmorillonite flocs flowing in a laminar shear flow. *Colloid Polym. Sci.* 297, 979–987. doi: 10.1007/s00396-019-04532-3

Ahrens, L., Taniyasu, S., Yeung, L. W. Y., Yamashita, N., Lam, P. K. S., and Ebinghaus, R. (2010). Distribution of polyfluoroalkyl compounds in water, suspended particulate matter and sediment from Tokyo Bay, Japan. *Chemosphere* 79, 266–272. doi: 10.1016/j.chemosphere.2010.01.045

Alldredge, A. L., and Gotschalk, C. C. (1989). Direct observations of the mass flocculation of diatom blooms: characteristics, settling velocities and formation of diatom aggregates. *Deep Sea Res. Part Oceanogr. Res. Pap.* 36, 159–171. doi: 10.1016/0198-0149(89)90131-3

Alldredge, A. L., Gotschalk, C. C., and MacIntyre, S. (1987). Evidence for sustained residence of macrocrustacean fecal pellets in surface waters off Southern California. *Deep Sea Res. Part Oceanogr. Res. Pap.* 34, 1641–1652. doi: 10.1016/0198-0149(87)90113-0

Alldredge, A. L., Granata, T. C., Gotschalk, C. C., and Dickey, T. D. (1990). The physical strength of marine snow and its implications for particle disaggregation in the ocean. *Limnol. Oceanogr.* 35, 1415–1428. doi: 10.4319/lo.1990.35.7.1415

Alldredge, A. L., and McGillivary, P. (1991). The attachment probabilities of marine snow and their implications for particle coagulation in the ocean. *Deep Sea Res. Part Oceanogr. Res. Pap.* 38, 431–443. doi: 10.1016/0198-0149(91)90045-H

Alldredge, A. L., Passow, U., and Haddock, H. D. (1998). The characteristics and transparent exopolymer particle (TEP) content of marine snow formed from thecate dinoflagellates. *J. Plankton Res.* 20, 393–406. doi: 10.1093/plankt/20.3.393

Alldredge, A. L., Passow, U., and Logan, B. E. (1993). The abundance and significance of a class of large, transparent organic particles in the ocean. *Deep Sea Res. Part Oceanogr. Res. Pap.* 40, 1131–1140. doi: 10.1016/0967-0637(93)90129-Q

Alldredge, A. L., and Silver, M. W. (1988). Characteristics, dynamics and significance of marine snow. *Prog. Oceanogr.* 20, 41–82. doi: 10.1016/0079-6611(88)90053-5

Blaser, S. (2002). Forces on the surface of small ellipsoidal particles immersed in a linear flow field. *Chem. Eng. Sci.* 57, 515–526. doi: 10.1016/S0009-2509(01)00389-X

Boller, M., and Blaser, S. (1998). Particles under stress. *Water Sci. Technol.* 37, 9–29. doi: 10.2166/wst.1998.0367

Boyd, P. W., Claustre, H., Levy, M., Siegel, D. A., and Weber, T. (2019). Multi-faceted particle pumps drive carbon sequestration in the ocean. *Nature* 568, 327–335. doi: 10.1038/s41586-019-1098-2

Briggs, N., Dall'Olmo, G., and Claustre, H. (2020). Major role of particle fragmentation in regulating biological sequestration of CO_2 by the oceans. *Science* 367, 791–793. doi: 10.1126/science.aay1790

Chen, C.-S., Shiu, R.-F., Hsieh, Y.-Y., Xu, C., Vazquez, C. I., Cui, Y., et al. (2021). Stickiness of extracellular polymeric substances on different surfaces via magnetic tweezers. *Sci. Total Environ.* 757, 143766. doi: 10.1016/j.scitotenv.2020.143766

Cruz, B. N., Brozak, S., and Neuer, S. (2021). Microscopy and DNA -based characterization of sinking particles at the Bermuda Atlantic Time-series Study station point to zooplankton mediation of particle flux. *Limnol. Oceanogr.* 66, 3697–3713. doi: 10.1002/lno.11910

Dilling, L., and Alldredge, A. L. (2000). Fragmentation of marine snow by swimming macrozooplankton: A new process impacting carbon cycling in the sea. *Deep Sea Res. Part Oceanogr. Res. Pap.* 47, 1227–1245. doi: 10.1016/S0967-0637(99)00105-3

Drapeau, D. T., Dam, H. G., and Grenie, G. (1994). An improved flocculator design for use in particle aggregation experiments. *Limnol. Oceanogr.* 39, 723–729. doi: 10.4319/lo.1994.39.3.0723

Droppo, I. G. (2004). Structural controls on floc strength and transport. *Can. J. Civ. Eng.* 31, 569–578. doi: 10.1139/l04-015

Duarte, C. M., Agustí, S., Vaqué, D., Agawin, N. S. R., Felipe, J., Casamayor, E. O., et al. (2005). Experimental test of bacteria-phytoplankton coupling in the Southern Ocean. *Limnol. Oceanogr.* 50, 1844–1854. doi: 10.4319/lo.2005.50.6.1844

Falkowski, P. (2012). Ocean Science: The power of plankton. *Nature* 483, S17–S20. doi: 10.1038/483S17a

Florio, B. J., Fawell, P. D., and Small, M. (2019). The use of the perimeter-area method to calculate the fractal dimension of aggregates. *Powder Technol.* 343, 551–559. doi: 10.1016/j.powtec.2018.11.030

Frappier, G., Lartiges, B. S., and Skali-Lami, S. (2010). Floc cohesive force in reversible aggregation: A couette laminar flow investigation. *Langmuir* 26, 10475–10488. doi: 10.1021/la9046947

Furukawa, K., and Okada, T. (2006). "Tokyo Bay: Its Environmental Status — Past, Present, and Future," in *The Environment in Asia Pacific Harbours*. Ed. E. Wolanski (Berlin/Heidelberg: Springer-Verlag), 15–34. doi: 10.1007/1-4020-3655-8_2

Furukawa, Y., Watkins, J. L., Kim, J., Curry, K. J., and Bennett, R. H. (2009). Aggregation of montmorillonite and organic matter in aqueous media containing artificial seawater. *Geochem. Trans.* 10, 2. doi: 10.1186/1467-4866-10-2

Goldthwait, S., Yen, J., Brown, J., and Alldredge, A. (2004). Quantification of marine snow fragmentation by swimming euphausiids. *Limnol. Oceanogr.* 49, 940–952. doi: 10.4319/lo.2004.49.4.0940

Goutx, M., Wakeham, S. G., Lee, C., Duflos, M., Guigue, C., Liu, Z., et al. (2007). Composition and degradation of marine particles with different settling velocities in the northwestern Mediterranean Sea. *Limnol. Oceanogr.* 52, 1645–1664. doi: 10.4319/lo.2007.52.4.1645

Hama, T., Inoue, T., Suzuki, R., Kashiwazaki, H., Wada, S., Sasano, D., et al. (2016). Response of a phytoplankton community to nutrient addition under different CO2 and pH conditions. *J. Oceanogr.* 72, 207–223. doi: 10.1007/s10872-015-0322-4

Hama, T., Kawashima, S., Shimotori, K., Satoh, Y., Omori, Y., Wada, S., et al. (2012). Effect ofocean acidification on coastal phytoplankton composition and accompanying organic nitrogen production. *J. Oceanogr.* 68, 183–194. doi: 10.1007/s10872-011-0084-6

Hill, P. (1998). Controls on floc size in the sea. *Oceanography* 11, 13–18. doi: 10.5670/oceanog.1998.03

Hill, P. S., Voulgaris, G., and Trowbridge, J. H. (2001). Controls on floc size in a continental shelf bottom boundary layer. *J. Geophys. Res. Oceans* 106, 9543–9549. doi: 10.1029/2000JC900102

IPCC AR6 (2021). "Climate change 2021: the physical science basis," in *Contribution of Working Group I to the Sixth Assessment Report of the Intergovernmental Panel on Climate Change*. Eds. V. Masson-Delmotte, P. Zhai, A. PIrani, S. L. Connors, C. Péan, S. Berger, N. Caud, Y. Chen, L. Goldfarb, M. I. Gomis, M. Huang, K. Leitzell, E. Lonnoy, J. B. R. Matthews, T. K. Maycock, T. Waterfield, O. Yelekci, R. Yu and B. Zhou (Cambridge: Cambridge University Press).

Irigoien, X., Klevjer, T. A., Røstad, A., Martinez, U., Boyra, G., Acuña, J. L., et al. (2014). Large mesopelagic fishes biomass and trophic efficiency in the open ocean. *Nat. Commun.* 5, 3271. doi: 10.1038/ncomms4271

Iseki, K., Whitney, F., and Wong, C. (1980). Biochemical changes of sedimented matter in sediment trap in shallow coastal waters. *Bull. Plankton Soc. Jpn.* 27, 27–36.

Jocher, G., Stoken, A., Borovec, J., NanoCode012, Stan, C., Changyu, L., et al. (2021). ultralytics/yolov5: v4.0 - nn.SiLU() activations, Weights & Biases logging, PyTorch Hub integration. *Zenodo*. doi: 10.5281/zenodo.4418161

Kahl, L., Vardi, A., and Schofield, O. (2008). Effects of phytoplankton physiology on export flux. *Mar. Ecol. Prog. Ser.* 354, 3–19. doi: 10.3354/meps07333

Kepkay, P. (1994). Particle aggregation and the biological reactivity of colloids. *Mar. Ecol. Prog. Ser.* 109, 293–304. doi: 10.3354/meps109293

Kobayashi, M. (2004). Breakup and strength of polystyrene latex flocs subjected to a converging flow. *Colloids Surf. Physicochem. Eng. Asp.* 235, 73–78. doi: 10.1016/j.colsurfa.2004.01.008

Kobayashi, M. (2005). Strength of natural soil flocs. *Water Res.* 39, 3273–3278. doi: 10.1016/j.watres.2005.05.037

Kobayashi, M., Adachi, Y., and Ooi, S. (1999). Breakup of fractal flocs in a turbulent flow. *Langmuir* 15, 4351–4356. doi: 10.1021/la980763o

Kowal, M., Żejmo, M., Skobel, M., Korbicz, J., and Monczak, R. (2020). Cell nuclei segmentation in cytological images using convolutional neural network and seeded watershed algorithm. *J. Digit. Imaging* 33, 231–242. doi: 10.1007/s10278-019-00200-8

Laurenceau-Cornec, E. C., Trull, T. W., Davies, D. M., Bray, S. G., Doran, J., Planchon, F., et al. (2015b). The relative importance of phytoplankton aggregates and zooplankton fecal pellets to carbon export: insights from free-drifting sediment trap deployments in naturally iron-fertilised waters near the Kerguelen Plateau. *Biogeosciences* 12, 1007–1027. doi: 10.5194/bg-12-1007-2015

Laurenceau-Cornec, E. C., Trull, T. W., Davies, D. M., Rocha, C. L. D. L., and Blain, S. (2015a). Phytoplankton morphology controls on marine snow sinking velocity. *Mar. Ecol. Prog. Ser.* 520, 35–56. doi: 10.3354/meps11116

Maggi, F. (2007). Variable fractal dimension: A major control for floc structure and flocculation kinematics of suspended cohesive sediment. *J. Geophys. Res.* 112, C07012. doi: 10.1029/2006JC003951

Mari, X., Passow, U., Migon, C., Burd, A. B., and Legendre, L. (2017). Transparent exopolymer particles: Effects on carbon cycling in the ocean. *Prog. Oceanogr.* 151, 13–37. doi: 10.1016/j.pocean.2016.11.002

Miyahara, K., Adachi, Y., Nakaishi, K., and Ohtsubo, M. (2002). Settling velocity of a sodium montmorillonite floc under high ionic strength. *Colloids Surf. Physicochem. Eng. Asp.* 196, 87–91. doi: 10.1016/S0927-7757(01)00798-1

Nayar, K. G., Sharqawy, M. H., Banchik, L. D., and Lienhard, V. ,. J. H. (2016). Thermophysical properties of seawater: A review and new correlations that include pressure dependence. *Desalination* 390, 1–24. doi: 10.1016/j.desal.2016.02.024

Oliver, R. L., Kinnear, A. J., and Ganf, G. G. (1981). Measurements of cell density of three freshwater phytoplankters by density gradient centrifugation1: Phytoplankton cell density. *Limnol. Oceanogr.* 26, 285–294. doi: 10.4319/lo.1981.26.2.0285

Parker, D., Kaufman, W. J., and Jenkins, D. (1972). Floc breakup in turbulent flocculation processes. *J. Sanit. Eng. Div.* 98, 79–99. doi: 10.1061/JSEDAI.0001389

Passow, U. (1991). Species-specific sedimentation and sinking velocities of diatoms. *Mar. Biol.* 108, 449–455. doi: 10.1007/BF01313655

Passow, U. (2000). Formation of transparent exopolymer particles, TEP, from dissolved precursor material. *Mar. Ecol. Prog. Ser.* 192, 1–11. doi: 10.3354/meps192001

Passow, U. (2002a). Production of transparent exopolymer particles (TEP) by phyto- and bacterioplankton. *Mar. Ecol. Prog. Ser.* 236, 1–12. doi: 10.3354/meps236001

Passow, U. (2002b). Transparent exopolymer particles (TEP) in aquatic environments. *Prog. Oceanogr.* 55, 287–333. doi: 10.1016/S0079-6611(02)00138-6

Passow, U., and Alldredge, A. L. (1995). Aggregation of a diatom bloom in a mesocosm: The role of transparent exopolymer particles (TEP). *Deep Sea Res. Part II Top. Stud. Oceanogr.* 42, 99–109. doi: 10.1016/0967-0645(95)00006-C

Passow, U., Alldredge, A. L., and Logan, B. E. (1994). The role of particulate carbohydrate exudates in the flocculation of diatom blooms. *Deep Sea Res. Part Oceanogr. Res. Pap.* 41, 335–357. doi: 10.1016/0967-0637(94)90007-8

Quigg, A., Santschi, P. H., Burd, A., Chin, W.-C., Kamalanathan, M., Xu, C., et al. (2021). From nano-gels to marine snow: A synthesis of gel formation processes and modeling efforts involved with particle flux in the ocean. *Gels* 7, 114. doi: 10.3390/gels7030114

Rohatgi, A. (2022) *Webplotdigitizer: Version 4.6*. Available at: https://automeris.io/WebPlotDigitizer.

Saffman, P. G., and Turner, J. S. (1956). On the collision of drops in turbulent clouds. *J. Fluid Mech.* 1, 16. doi: 10.1017/S0022112056000020

Schindelin, J., Arganda-Carreras, I., Frise, E., Kaynig, V., Longair, M., Pietzsch, T., et al. (2012). Fiji: an open-source platform for biological-image analysis. *Nat. Methods* 9, 676–682. doi: 10.1038/nmeth.2019

Sharqawy, M. H., Lienhard, J. H., and Zubair, S. M. (2010). Thermophysical properties of seawater: a review of existing correlations and data. *Desalination Water Treat.* 16, 354–380. doi: 10.5004/dwt.2010.1079

Shimotori, K., Omori, Y., and Hama, T. (2009). Bacterial production of marine humic-like fluorescent dissolved organic matter and its biogeochemical importance. *Aquat. Microb. Ecol.* 58, 55–66. doi: 10.3354/ame01350

Siegel, D. A., Buesseler, K. O., Doney, S. C., Sailley, S. F., Behrenfeld, M. J., and Boyd, P. W. (2014). Global assessment of ocean carbon export by combining satellite observations and food-web models. *Glob. Biogeochem. Cycles* 28, 181–196. doi: 10.1002/2013GB004743

Smith, D. C., Steward, G. F., Long, R. A., and Azam, F. (1995). Bacterial mediation of carbon fluxes during a diatom bloom in a mesocosm. *Deep Sea Res. Part II Top. Stud. Oceanogr.* 42, 75–97. doi: 10.1016/0967-0645(95)00005-B

Son, M., and Hsu, T.-J. (2009). The effect of variable yield strength and variable fractal dimension on flocculation of cohesive sediment. *Water Res.* 43, 3582–3592. doi: 10.1016/j.watres.2009.05.016

Song, Y., and Rau, M. J. (2022). A novel method to study the fragmentation behavior of marine snow aggregates in controlled shear flow. *Limnol. Oceanogr. Methods* 20, 618–632. doi: 10.1002/lom3.10509

Soos, M., Moussa, A. S., Ehrl, L., Sefcik, J., Wu, H., and Morbidelli, M. (2008). Effect of shear rate on aggregate size and morphology investigated under turbulent conditions in stirred tank. *J. Colloid Interface Sci.* 319, 577–589. doi: 10.1016/j.jcis.2007.12.005

Spinewine, B., Capart, H., Larcher, M., and Zech, Y. (2003). Three-dimensional Voronoï imaging methods for the measurement of near-wall particulate flows. *Exp. Fluids* 34, 227–241. doi: 10.1007/s00348-002-0550-4

Suzuki, R., and Ishimaru, T. (1990). An improved method for the determination of phytoplankton chlorophyll using N, N-dimethylformamide. *J. Oceanogr. Soc Jpn.* 46, 190–194. doi: 10.1007/BF02125580

Takeuchi, M., Doubell, M. J., Jackson, G. A., Yukawa, M., Sagara, Y., and Yamazaki, H. (2019). Turbulence mediates marine aggregate formation and destruction in the upper ocean. *Sci. Rep.* 9, 1–8. doi: 10.1038/s41598-019-52470-5

Thornton, D. C. O. (2002). Diatom aggregation in the sea: mechanisms and ecological implications. *Eur. J. Phycol.* 37, 149–161. doi: 10.1017/S0967026202003657

Turner, J. (2002). Zooplankton fecal pellets, marine snow and sinking phytoplankton blooms. *Aquat. Microb. Ecol.* 27, 57–102. doi: 10.3354/ame027057

Turner, J. T. (2015). Zooplankton fecal pellets, marine snow, phytodetritus and the ocean's biological pump. *Prog. Oceanogr.* 130, 205–248. doi: 10.1016/j.pocean.2014.08.005

Uchimiya, M., Fukuda, H., Wakita, M., Kitamura, M., Kawakami, H., Honda, M. C., et al. (2018). Balancing organic carbon supply and consumption in the ocean's interior: Evidence from repeated biogeochemical observations conducted in the subarctic and subtropical western North Pacific. *Limnol. Oceanogr.* 63, 2015–2027. doi: 10.1002/lno.10821

Usher, W., Herman, J., Whealton, C., Hadka, D., Xantares, Rios, F., et al. (2016). Salib/salib: launch!. *Zenodo*. doi: 10.5281/ZENODO.160164

van der Walt, S., Schönberger, J. L., Nunez-Iglesias, J., Boulogne, F., Warner, J. D., Yager, N., et al. (2014). scikit-image: Image processing in python. *PeerJ* 2, e453. doi: 10.7717/peerj.453

Verspagen, J., Visser, P., and Huisman, J. (2006). Aggregation with clay causes sedimentation of the buoyant cyanobacteria Microcystis spp. *Aquat. Microb. Ecol.* 44, 165–174. doi: 10.3354/ame044165

Welschmeyer, N. A. (1994). Fluorometric analysis of chlorophyll a in the presence of chlorophyll b and pheopigments. *Limnol. Oceanogr.* 39, 1985–1992. doi: 10.4319/lo.1994.39.8.1985

Winterwerp, J. C. (1998). A simple model for turbulence induced flocculation of cohesive sediment. *J. Hydraul. Res.* 36, 309–326. doi: 10.1080/00221689809498621

Yamada, Y., Fukuda, H., Tada, Y., Kogure, K., and Nagata, T. (2016). Bacterial enhancement of gel particle coagulation in seawater. *Aquat. Microb. Ecol.* 77, 11–22. doi: 10.3354/ame01784

Yoon, W., Kim, S., and Han, K. (2001). Morphology and sinking velocities of fecal pellets of copepod, molluscan, euphausiid, and salp taxa in the northeastern tropical Atlantic. *Mar. Biol.* 139, 923–928. doi: 10.1007/s002270100630

Yuan, Y., and Farnood, R. R. (2010). Strength and breakage of activated sludge flocs. *Powder Technol.* 199, 111–119. doi: 10.1016/j.powtec.2009.11.021